

A spectral boundary integral method for inviscid water waves in a finite domain

J.S. Im and J. Billingham*

School of Mathematical Sciences, The University of Nottingham, University Park, Nottingham NG7 2RD, UK

SUMMARY

In this paper we show how the spectral formulation of Baker, Meiron and Orszag can be used to solve for waves on water of infinite depth confined between two flat, vertical walls, and also how it can be modified to take into account water of finite depth with a spatially-varying bottom. In each case, we use Chebyshev polynomials as the basis of our representation of the solution and filtering to remove spurious high-frequency modes. We show that spectral accuracy can be achieved until wave breaking, plunging or wall impingement occurs in two model problems. Copyright © 2015 John Wiley & Sons, Ltd.

Received ...

KEY WORDS: spectral method, boundary integral method, water waves

1. INTRODUCTION

Since the seminal work presented in [1], two-dimensional, nonlinear, inviscid water wave problems have usually been solved using a mixed Eulerian-Lagrangian formulation in conjunction with a boundary integral method to solve Laplace's equation. Other examples include [2], [3], [4], [5] and [6]. The most accurate version of this method is spectral, but has previously only been formulated for periodic problems. In this paper we show how the spectral formulation of [7] can be used to solve for waves on water of infinite depth confined between two flat, vertical walls, and also how it can be modified to take into account water of finite depth with a spatially-varying bottom. In each case, we use Chebyshev polynomials as the basis of our representation of the solution and filtering to remove spurious high-frequency modes. We show that spectral accuracy can be achieved until either wave breaking, plunging or wall impingement occurs in two model problems. Our focus is on the technical details of this numerical method, not the fluid mechanics, which will be addressed in a separate paper.

2. MATHEMATICAL FORMULATION

2.1. Governing equations

We consider the two-dimensional flow of an inviscid, incompressible fluid confined between two parallel, vertical walls. We non-dimensionalize the problem using the distance between the walls and the acceleration due to gravity to provide length and time scales. Let the horizontal and vertical coordinates be x and y . The walls are located at $x = 0$ and $x = \pi$ (for convenience in the presentation

*Correspondence to: School of Mathematical Sciences, The University of Nottingham, University Park, Nottingham NG7 2RD, UK. E-mail: John.Billingham@Nottingham.ac.uk

below). The free surface at time t is $y = \eta(x, t)$ [†]. We assume that the fluid motion is irrotational, so that there exists a velocity potential $\phi(x, y, t)$. We also assume incompressibility of the fluid, so that ϕ satisfies Laplace's equation,

$$\nabla^2 \phi = 0 \text{ in } y < \eta(x, t), \quad 0 \leq x \leq \pi. \quad (1)$$

On the free surface, we have the kinematic and dynamic boundary conditions,

$$\eta_t + \phi_x \eta_x - \phi_y = 0 \text{ on } y = \eta(x, t), \quad (2)$$

$$\phi_t + \frac{1}{2}(\phi_x^2 + \phi_y^2) + y = 0 \text{ on } y = \eta(x, t). \quad (3)$$

The effect of surface tension has been neglected. We assume that the flow is on a large enough scale that this is appropriate, although we expect surface tension to become important once a wave starts to break since the free surface then develops a large curvature, possibly becoming singular at some finite time, [8], [9]. Gravity acts in the negative y direction. Since the rigid parallel walls are located at $x = 0$ and $x = \pi$, the potential needs to satisfy the homogeneous Neumann boundary conditions

$$\frac{\partial \phi}{\partial x} = 0 \text{ at } x = 0, \quad x = \pi. \quad (4)$$

Equations (1), (2), (3) and (4), along with appropriate initial conditions for ϕ and η , govern the motion of the fluid.

2.2. Boundary integral formulation on water of infinite depth

As shown in many previous works on water wave problems, the most computationally effective way to solve Laplace's equation (1) is the boundary integral method, which reduces the problem to one formulated on the free surface alone. A formulation based on classical potential theory [10], [11] uses dipole distributions along the free surface and this is the basis of our numerical method. This particular choice of boundary integral method was used for the first time in [7], for spatially periodic waves.

Let $z = x + iy$ be a complex-valued field point and introduce parametric forms for the surface location $z(p)$ with dipole distribution $\mu(p)$ where p is a Lagrangian parameter defined in $[0, \pi]$. Then the complex potential $\Phi = \phi + i\psi$ has a double-layer representation

$$\Phi(z) = \frac{1}{4\pi i} \int_0^\pi \mu(q) [z_q(q) \cot \frac{1}{2}(z - z(q)) + z_q^*(q) \cot \frac{1}{2}(z + z^*(q))] dq, \quad (5)$$

where ϕ is the velocity potential and ψ the stream function. Here we drop the time variable for convenience. The subscript q denotes differentiation with respect to q and the $*$ superscript indicates complex conjugation. This automatically satisfies the kinematic boundary condition since the double-layer representation implies the continuity of the normal derivative of the potential at the interface. If we take the limit as z approaches the free surface from below, $\Phi(z) \rightarrow \Phi(z(p)) = \Phi(p)$ and the integral should be understood as a principal value integral. In addition, we de-singularize the integrand for numerical purposes and obtain

$$\begin{aligned} \Phi(p) &= \frac{1}{4\pi i} \text{P.V.} \int_0^\pi (\mu(q) - \mu(p)) [z_q(q) \cot \frac{1}{2}(z - z(q)) + z_q^*(q) \cot \frac{1}{2}(z + z^*(q))] dq + \frac{\mu(p)}{2} \\ &\equiv I(p; \mu) + \frac{\mu(p)}{2}. \quad (6) \end{aligned}$$

[†] We will later adopt a Lagrangian representation of the free surface, so we should not be concerned by the possibility of η becoming multivalued.

The complex velocity $w = u + iv$, where u and v are the x and y components of velocity respectively, is given by

$$w^*(z) = \frac{\partial \Phi}{\partial z}, \quad (7)$$

and the velocity of the free surface parametrized by p is determined by

$$w^*(p) = \frac{\Phi_p(p)}{z_p(p)}. \quad (8)$$

The Lagrangian motion of the fluid particles on the free surface, keeping p fixed, is determined by

$$\frac{\partial z}{\partial t}(p) = w(p). \quad (9)$$

Bernoulli's equation determines the evolution of the potential in time on the free surface as

$$\frac{\partial \phi}{\partial t}(p) = \frac{1}{2}(u(p)^2 + v(p)^2) - y(p), \quad (10)$$

where p is fixed. In addition, (6) provides a Fredholm integral equation of the second kind for the dipole strength μ ,

$$\mu(p) = 2\phi(p) - \text{Re} \{I(p; \mu)\}. \quad (11)$$

If z and ϕ are given at a certain time t , we first solve the Fredholm integral equation (11) to determine the dipole strength μ , then the complex potential Φ can be determined from (6) and the complex velocity can be calculated using (8). Finally, the surface location and velocity potential on the free surface can be updated using (9) and (10), respectively. The process is repeated with the updated free surface z and surface potential ϕ .

2.3. Inclusion of bottom topography

Modelling surface waves over water of finite depth with spatially varying bottom topography requires an additional Neumann boundary condition along the rigid bottom. We define the dipole strengths along the free surface and rigid bottom to be μ_F and μ_B , and the parametrization of the surface and the rigid bottom to be z_F and z_B . The equivalent of (5) is then

$$\begin{aligned} \Phi(x, y) = & \frac{1}{4\pi i} \int_0^\pi \mu_F(q) \left\{ z_{F,q}(q) \cot \frac{1}{2}(z - z_F(q)) + z_{F,q}^*(q) \cot \frac{1}{2}(z + z_F^*(q)) \right\} dq \\ & + \frac{1}{4\pi} \int_0^\pi \mu_B(q) \left\{ z_{B,q}(q) \cot \frac{1}{2}(z - z_B(q)) - z_{B,q}^*(q) \cot \frac{1}{2}(z + z_B^*(q)) \right\} dq. \end{aligned}$$

After it has been desingularized, this can be solved in the same manner as described in section 2.2.

3. NUMERICAL METHOD

We use the Chebyshev polynomials, T_k , as the basis for the approximation of the solution, expressing each of the variables $\xi = \{x, y, \phi, \psi, \mu\}$ in the form

$$\xi(p) = \sum_{k=0}^N A_k T_k\left(\frac{2}{\pi}p - 1\right) \quad \text{for } p \in [0, \pi], \quad (12)$$

where N is the number of Lagrangian marker points on the free surface. By taking $\frac{2}{\pi}p - 1 = \cos \theta$ and defining Chebyshev nodes p_i corresponding to $\theta_i = i\frac{\pi}{N}$, we can use the Fast Cosine Transform

to determine the coefficient A_k [12] for given values $\xi(p_i)$. The derivatives of ξ are then

$$\xi_p(p) = \frac{2}{\pi} \sum_{k=0}^N B_k T_k\left(\frac{2}{\pi}p - 1\right) \quad (13)$$

where

$$B_{2k} = 2 \sum_{j=k}^{(N-1)/2} (2j+1)A_{2j+1} \text{ for } k \geq 1, \quad B_{2k+1} = 2 \sum_{j=k+1}^{N/2} (2j)A_{2j} \text{ for } k \geq 0,$$

$$B_0 = \sum_{j=0}^{(N-1)/2} (2j+1)A_{2j+1}. \quad (14)$$

Once the coefficients, B_k , are computed, the inverse Fast Cosine Transform gives the derivatives at the markers.

Since Chebyshev polynomials are used as the basis and the marker points are placed at the Chebyshev nodes, a natural choice of quadrature rule is the Clenshaw-Curtis method [13]. This requires the evaluation of the integrand at the Chebyshev nodes in order to approximate the integrand by Chebyshev polynomials. The integral can then be determined exactly with the Fourier Cosine Transform. To explain in more detail, first consider a change of variable, $\cos \theta = \frac{2}{\pi}p - 1$, which gives

$$\int_0^\pi f(p) dp = \frac{\pi}{2} \int_0^\pi f\left(\frac{\pi}{2}(\cos \theta + 1)\right) \sin \theta d\theta. \quad (15)$$

Application of the Fast Cosine Transform to $f\left(\frac{\pi}{2}(\cos \theta + 1)\right)$ determines the coefficients, so that

$$f\left(\frac{\pi}{2}(\cos \theta + 1)\right) = \sum_{k=0}^N A_k \cos(k\theta), \quad (16)$$

and hence

$$\int_0^\pi f(p) dp = \sum_{k=0}^{N/2} \frac{2A_{2k}}{1 - (2k)^2}. \quad (17)$$

In addition, the value of the integrand in (6) at the removable singularity is given by a limiting value $i\mu_p(p)/(2\pi)$ as $q \rightarrow p$ and this value is used to approximate the integrand with Chebyshev polynomials.

It remains to determine the dipole strength μ . A very efficient iterative method,

$$\mu^{(n+1)}(p) = 2\phi(p) - \text{Re}\{I(p, \mu^{(n)})\}, \quad (18)$$

can be applied to (11), and convergence is guaranteed, as shown in [7]. We stop this iteration when the absolute difference between successive iterates is less than an error tolerance. For time integration, we use an explicit fourth-order Runge-Kutta method. We also filter the solution to suppress high order modes in the Chebyshev series approximation, [14]. Because of the unevenly distributed marker points and explicit time integration method, a small time step is required for stability.

In order to investigate the accuracy of our method, note that the total perturbation energy is

$$E = \frac{1}{2}g \int_0^\pi y(q)^2 x_q(q) dq + \frac{1}{2} \int_0^\pi \phi_q(q) \psi(q) dq, \quad (19)$$

which is conserved in time. We can calculate this integral numerically using the Clenshaw-Curtis method. The total perturbation energy $E(t)$ is used to monitor the number of digits of accuracy in the fractional change of energy, namely

$$-\log_{10} \left(\left| \frac{E(t) - E(0)}{E(0)} \right| \right). \quad (20)$$

4. NUMERICAL RESULTS

In order to demonstrate our method, we consider two test problems: firstly, a collapsing wave in fluid of infinite depth, which illustrates the development of both spilling breakers and plunging jets, and secondly waves in fluid of finite depth, either of uniform depth or running along a ramped bottom, which illustrates rising jet formation, air entrainment and flip through.

4.1. Unsteady spilling breaker and plunging jet formation in water of infinite depth

We use initial conditions

$$\begin{aligned} x(p) &= p, \\ y(p) &= \epsilon \left(\frac{2}{\pi^4} (x(p)^2 - \pi^2)^2 - 1 \right) \equiv \frac{\epsilon}{8} \left[\frac{3}{8} T_0(\zeta) - 9T_1(\zeta) - \frac{1}{2} T_2(\zeta) + T_3(\zeta) + \frac{1}{8} T_4(\zeta) \right], \\ \phi(p) &= 0, \end{aligned}$$

where $\zeta = \frac{2}{\pi}p - 1$ and T_k is a Chebyshev polynomial. The initial, stationary position of the free surface is a symmetric, quartic polynomial, elevated to height $\epsilon > 0$ at $x = 0$ and depressed to depth $-\epsilon$ at $x = \pi$. Note that, although this is qualitatively similar to $\eta(x, 0) = \epsilon \cos x$, its periodic extension is not infinitely differentiable, and therefore cannot be used as the initial condition for a periodic spectral solver. Note also that the initial condition satisfies $\eta_x(0, 0) = \eta_x(\pi, 0) = 0$. The slope of the free surface at the walls remains zero for $t > 0$. If the initial condition does not satisfy these zero slope conditions, the flow develops a small scale structure close to each wall that is not readily computed using a global method such as ours (see [15] for a related example). The number of digits of accuracy rapidly becomes small in this case.

As a simple test, we take $\epsilon = 0.5$ as an initial condition and use various time steps, dt , and fix $N = 256$ and also various numbers of markers, N , and fix $dt = \pi/128$, and integrate until $t = 2\pi$. Figure 1 shows the number of digits of accuracy in the fractional change of the total energy for various time steps. The energy has about 7 digits of accuracy or better depending on the step size. The results shown in Table I confirm that our time stepping method works correctly since the error decreases by a factor of 1/16 when we halve the time step. Table II shows a large decrease of the numerical error as N increases, consistent with spectral accuracy.

Table I. Numerical error in time : $\epsilon = .5$, $N = 256$

dt	$\ln x(2\pi)$	$\ln y(2\pi)$	$\ln \phi(2\pi)$
$\pi/256$	1.917159e-07	1.109367e-07	9.315433e-08
$\pi/512$	3.385032e-08	2.834658e-08	5.275946e-09

Table II. Numerical error in space : $\epsilon = .5$, $dt = \pi/128$

N	$\ln x(2\pi)$	$\ln y(2\pi)$
64	4.511496e-03	3.554278e-03
128	2.498743e-05	1.961779e-05
256	9.088917e-07	9.197125e-07

For small values of the amplitude, $\epsilon \leq 0.4$, we obtain close to linear waves, which slosh back and forth without breaking. For larger values of ϵ , we observe breaking waves. We first consider the case $\epsilon = 0.45$. We increased the spatial and temporal resolution to $N = 512$ and $\Delta t = 1/1024$ from $t = 7$ to $t = 8$, and $\Delta t = 1/4096$ from $t = 8$ to $t = 9$ to accurately capture the breaking wave. The magnitude of spectrum below 10^{-13} is suppressed by the filter and the tolerance level for the

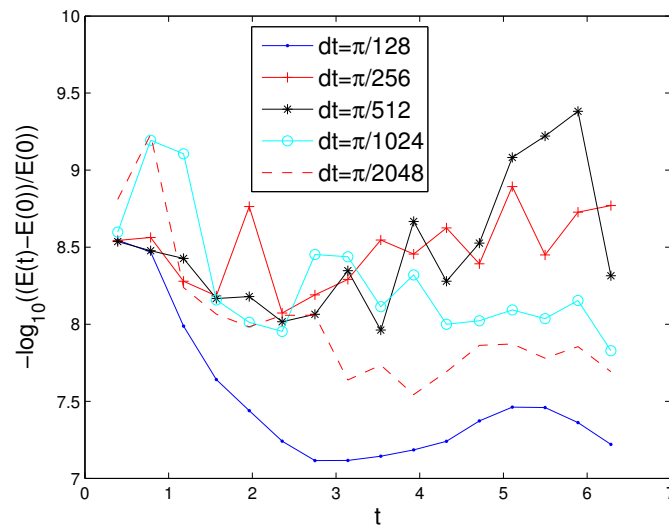


Figure 1. Number of digits of accuracy, $N = 256$, $\epsilon = 0.5$.

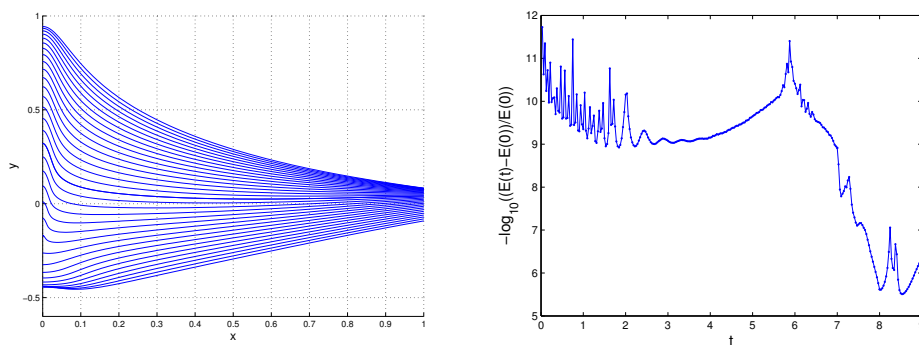


Figure 2. (Left) Profiles near the wall in the collapsing peak from $t = 7$ to $t = 9$ in increments of 0.02π for $\epsilon = 0.45$, (Right) Number of accurate digits in the total energy.

iterative method is 10^{-12} . This filter level and tolerance level are used in all the simulations in this paper. The results are plotted in Figure 2. The profile in Figure 2 shows a collapsing peak. As the peak collapses, it sharpens and the simulation requires smaller time steps while the number of digits of accuracy decreases from $t = 7$ to $t = 9$. Eventually, the peak disappears and the profile flips over. Similar behavior was seen by Baker and Xie in [8] with a sinusoidal initial condition. As the trough of the profile reaches its lowest point, it flips over once again and develops a crest. Further simulation results are shown in Figure 3. The resolution is set to $N = 1024$ and $\Delta t = 1/4096$. As the tip of the crest sharpens, it requires more markers on the free surface. A mass of water then moves away from the wall, a sharp tip forms on the free surface and a plunging breaker is generated.

We now consider the solution when $\epsilon = 0.55$. Figure 4 shows the wave profiles from $t = 5$ to $t = 5.40$ and its enlarged view shows the formation of a plunging breaker. The resolution is set as $N = 1024$ and $\Delta t = 1/4000$. The curvature profiles in Figure 5 show an exponential increase at the tip of the surface as the profile turns over. This is clear evidence of a plunging breaker. In addition, the number of digits in the fractional change of the total energy is shown and indicates that at least 7 digits are accurate. Figure 6 shows the spectrum of the profile in the wave number k plotted at $t = 5.3875$ and $t = 5.4$. Although the wave steepens and forms a sharp tip on the free surface, the spectra show that the numerical solution remains stable.

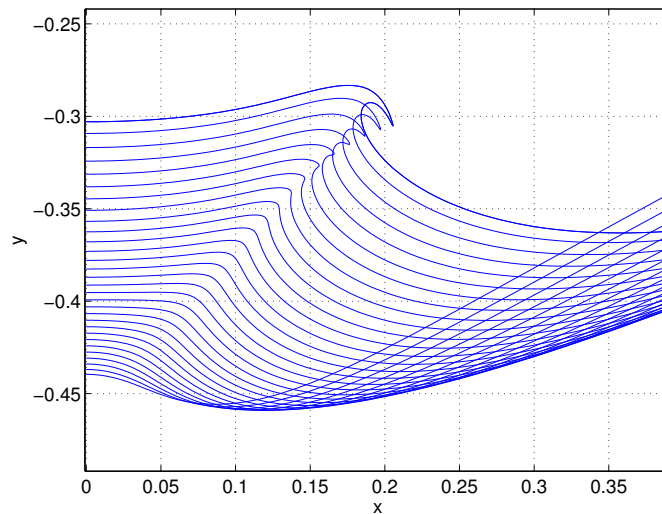


Figure 3. Profiles of breaking waves near the wall from $t = 9$ to $t = 9.9$ for $\epsilon = 0.45$

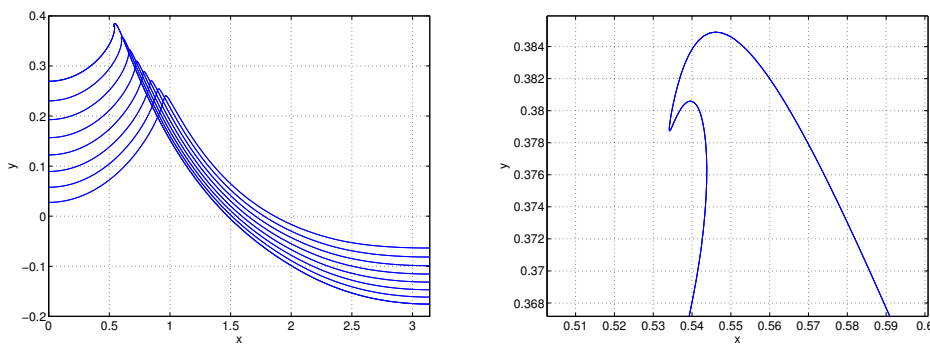


Figure 4. (Left) Sequence of profiles from $t = 5$ to $t = 5.40$, (Right) Enlarged view near the tip of the plunging jet at $t = 5.40$ for $\epsilon = 0.55$

When $\epsilon = 0.5385$, we were able to observe a spilling breaker, shown in Figure 7. The amplitude in this case is slightly smaller than that which generated a plunging breaker. The resolution is set to $N = 1024$ and $\Delta t = 1/65536$. We see that the curvature becomes large in both positive and negative senses, in contrast to the plunging breaker, where the large curvature is purely negative. We would expect that surface tension leads to the generation of a capillary wave on the underside of the spilling breaker if it were to be included in the simulation, see for example, [3], [9]. The shortest distance between the wall at $x = 0$ and profile is approximately 0.00005. We could not proceed further with the simulation, since the profile almost touches the wall. For $\epsilon \geq .6$, the wave always breaks, and the breaking time gets earlier as ϵ increases. Figure 8 shows a series of profiles as a breaking wave is formed from the edge of a crest. The energy has eight digits of accuracy. For $\epsilon = 1$ and $\epsilon = 2$, as shown in Figure 9, the tip of the breaking wave is formed close to the other wall, $x = \pi$.

4.2. Wave breaking in water of finite depth

We begin by considering water of uniform depth d , and initial conditions

$$x_F(p) = p, \quad y_F(0) = \eta = \epsilon \tanh \left[R \left(x_F - \frac{L}{2} \right) \right], \quad \phi_F(p) = 0. \quad (21)$$

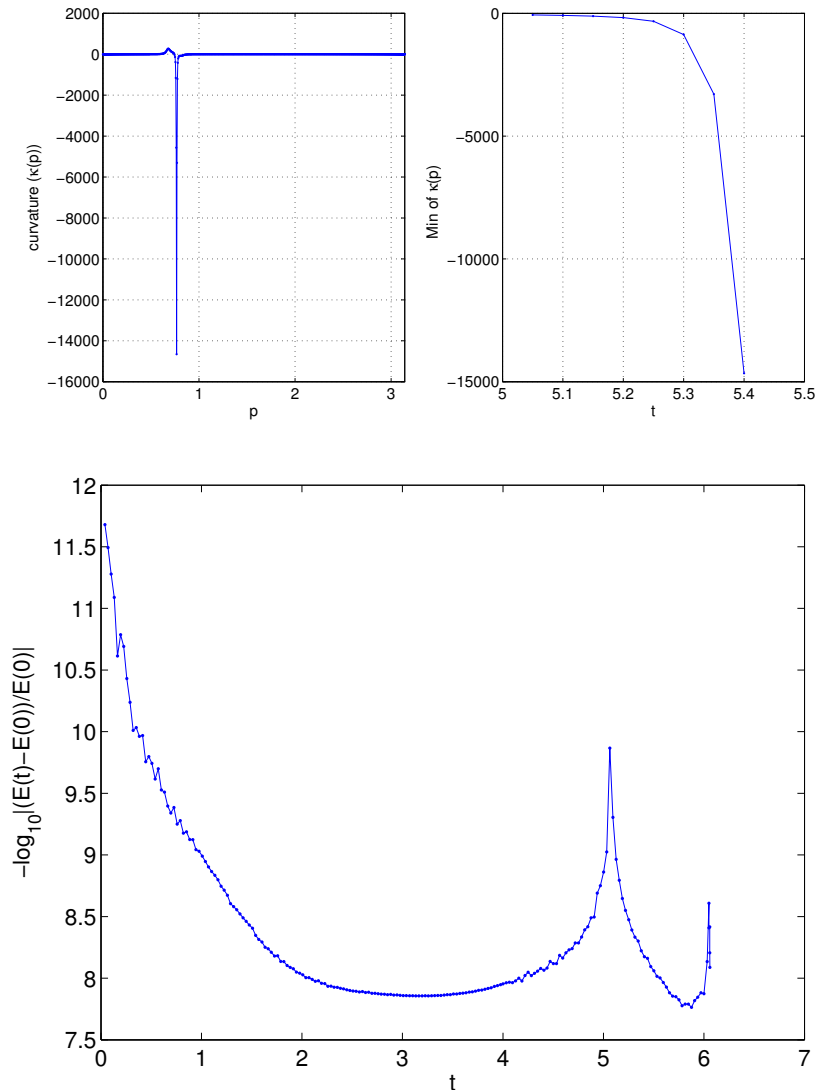


Figure 5. (1) Curvature at $t = 5.40$, (2) The minimum of curvature in time, (3) Numbers of digits in the fractional change of the total energy in time for $\epsilon = 0.55$

A simulation with this initial condition can be found in [5] which describes a desingularized integral equation technique. We take $\epsilon = 0.39$, $R = 3.06$ and $d = 0.59$, and set $L = \pi$ to place the largest initial slope of the free surface in the middle of the domain. Figure 10 shows both our numerical solution and the equivalent result shown in Figure 13 from [5]. The green line in [5] visually agrees well with our numerical results. In order to further check our numerical method, we performed resolution studies in time and space, with the results shown in Tables III and IV, which confirm that the method is fourth order in time, as it is for the case of fluid of infinite depth discussed above.

Now we consider a rigid bottom with a slope, so that

$$x_B(p) = p, \quad y_B(p) = -d + ax_B(p).$$

The results with the initial condition given in (21) and different bottom geometries, $a = -0.1$ and $a = 0.1$, are shown at the same time in Figure 11 and Figure 12, respectively. Figure 11 shows the sequence of profiles as the water runs up the slope so that a jet flips through and is projected up the wall at $x = 0$. As the jet climbs up the wall, the velocity of the contact point is approximately

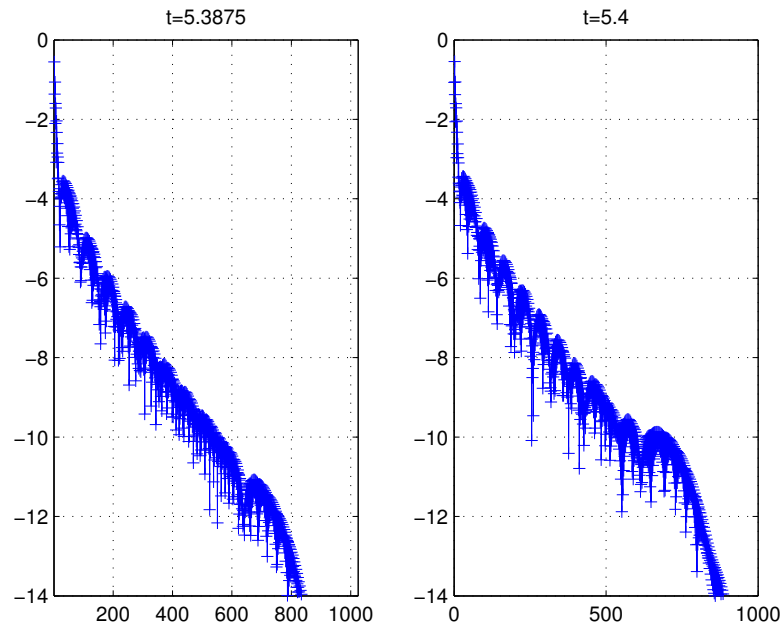


Figure 6. Spectrum of profiles ($\log_{10} \hat{y}_k$) at $t = 5.3875$ and $t = 5.4$ for $\epsilon = 0.55$

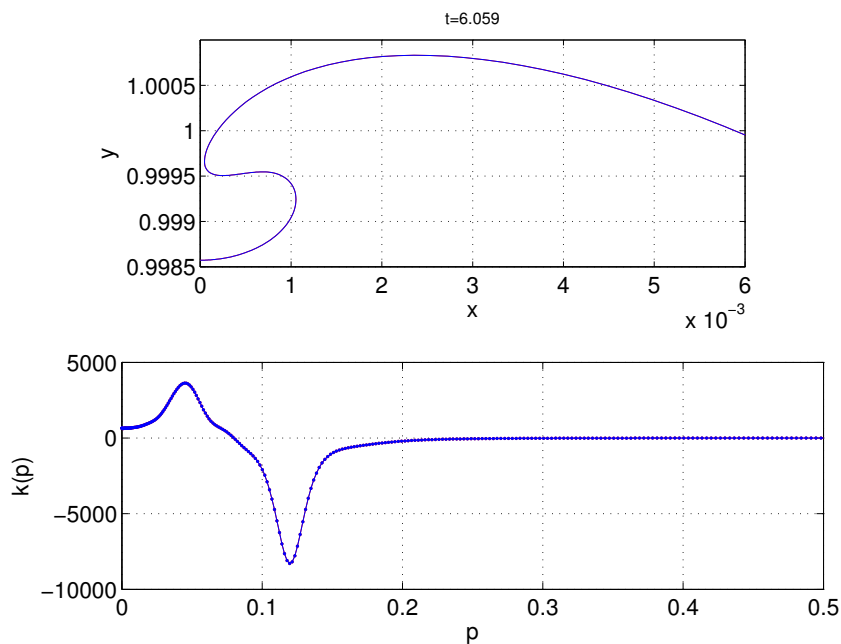


Figure 7. (Top) Enlarged view of the profile near the wall and (Bottom) curvature $\kappa(p)$ versus p at $t = 6.059$ for $\epsilon = 0.5385$.

constant, as is the width of the crest. In contrast, with $a = 0.1$, Figure 12 shows that as the water flows down the slope, a pocket is formed as the wave approaches the wall.

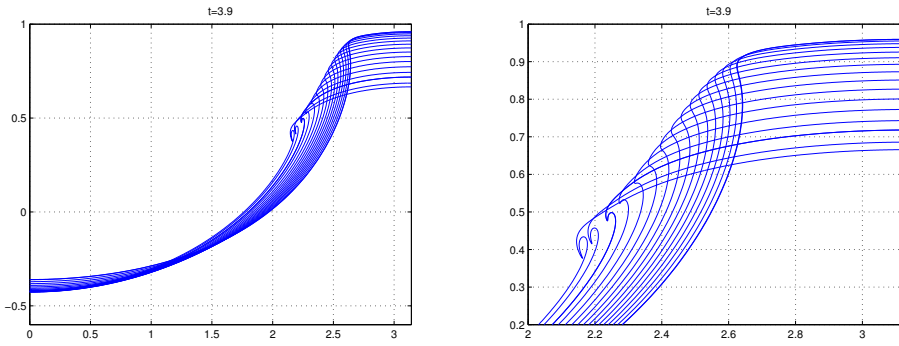


Figure 8. Left : Free surface profile, $N = 1024$, $dt = 1/4096$, Right : Enlarged view, $\epsilon = 0.70$.

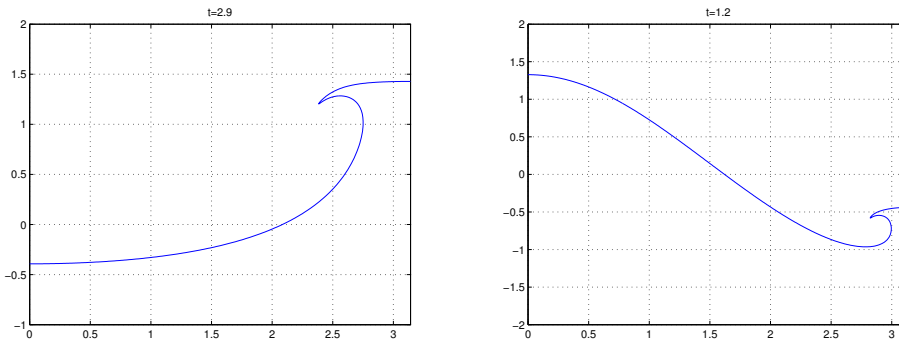


Figure 9. Left : Free surface profile for $\epsilon = 1$ at $t = 2.90$, $N = 512$, $dt = 1/256$, Right: Free surface profile for $\epsilon = 2$ at $t = 1.20$, $N = 1024$, $dt = 1/1024$

Table III. Resolution study in time : $N = 128$, $t = 0.62s$

dt	Num. Error in x_F	Num. Error in y_F	Num. Error in ϕ_F
$\pi/128$	5.006841e-06	4.866769e-06	4.783611e-06
$\pi/256$	4.852808e-07	4.215590e-07	4.744675e-07
$\pi/512$	2.971162e-08	2.374861e-08	2.908782e-08
$\pi/1024$	1.680888e-09	1.482410e-09	1.641206e-09

Table IV. Resolution study in space : $dt = \pi/512$, $t = 0.62s$

N	Num. Error in x_F	Num. Error in y_F
128	1.662461e-03	9.554908e-04
256	5.871008e-06	2.897034e-06
512	8.468930e-07	2.545283e-07

We also considered the case of a bottom surface with a tanh profile and with a fourth order polynomial initial condition,

$$x_f(p) = p, \quad y_f(p) = \epsilon \left(\frac{2}{\pi^4} (p^2 - \pi^2) \right)^2 - 1, \quad \phi_f(p) = 0$$

$$x_b(p) = p, \quad y_b(p) = -d + a \tanh\left(\left(p - \frac{\pi}{2}\right)/c\right)$$

We took $\epsilon = 0.4$, $d = 0.7$ for the initial profile and $c = 0.5$ and $a = \pm 0.1$ for the rigid bottom, with results shown in Figure 13. We can see that one bottom generates a spilling breaker and the other a plunging jet.

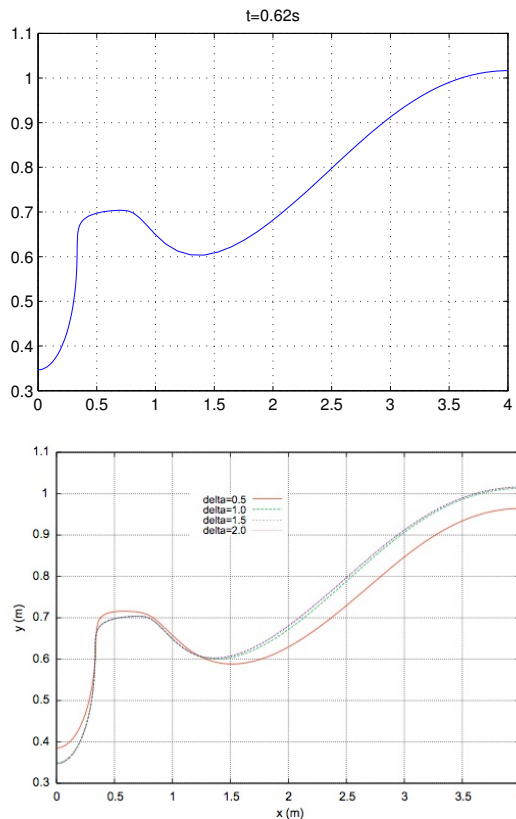


Fig. 13. Free surface profiles computed at $t = 0.62$ s for varying values of $\delta \in [0.5 : 2]$. The initial condition is defined by Eq. (24) and parameters $A = 0.495$ m, $h = 0.75$ m, $R = 2.4$ and $L = 4$ m.

Figure 10. Comparison of our computed free surface profile with the result in [5]: $N = 128$, $dt = \pi/64$, $t = 0.62$ s, $\epsilon = 0.39$, $R = 3.06$, $d = 0.59$

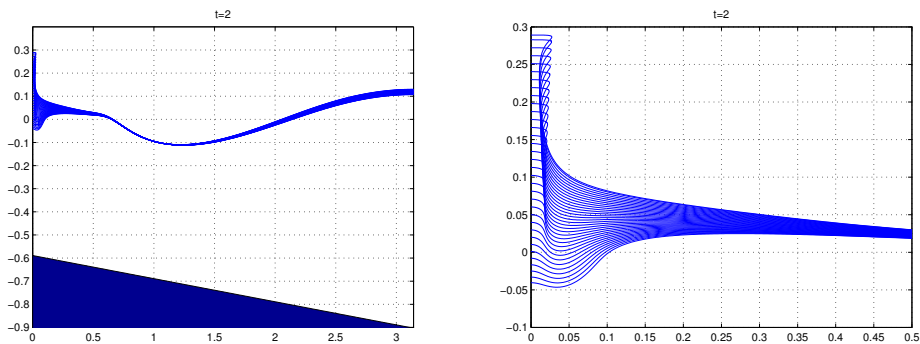


Figure 11. Free surface profile in flow up a ramp, $N = 512$, $dt = \pi/16384$, $t = 2.00$, $\epsilon = 0.39$

5. CONCLUSIONS

In this paper, we have shown that a spectral boundary integral method can be used to solve inviscid water wave problems in a finite domain, both with and without bottom topography. We were able to achieve spectral accuracy and conserve energy to eight decimal places until wave breaking occurred, accurately simulating breaking waves of various types, consistent with previous studies both in both finite domains and unbounded, spatially-periodic domains. In future work, we will extend this method to include the effect of surface tension, a problem made more challenging than the periodic

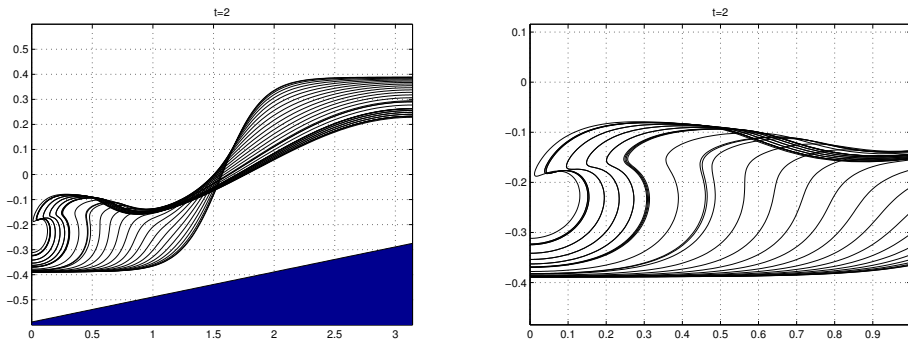


Figure 12. Free surface profile in flow down a ramp, $N = 256$, $dt = \pi/128$, $t = 2.00$, $\epsilon = 0.39$

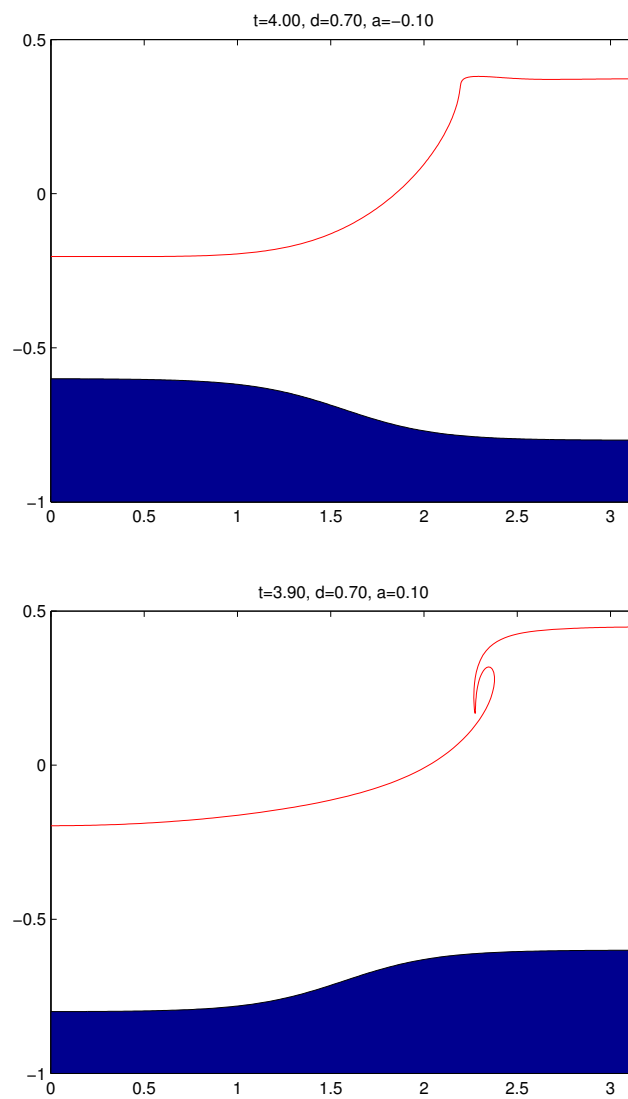


Figure 13. The effect of bottom topography on a breaking wave.

problem, studied in [3] and [6], by the need to apply an additional boundary condition at the moving contact lines on the rigid walls.

ACKNOWLEDGEMENTS

This work was funded by the UK Engineering and Physical Sciences Research Council through grant EP/H007830/1.

REFERENCES

1. Longuet-Higgins M, Cokelet E. The deformation of steep surface waves on water. i a numerical method of computation. *Proc. R. Soc. Lond. A* 1976; **350**:1–26.
2. Dold JW. An efficient surface-integral algorithm applied to unsteady gravity waves. *J. Comput. Phys.* 1992; **103**(1):90–115.
3. Ceniceros HD, Hou TY. Dynamic generation of capillary waves. *Phys. Fluids* 1999; **11**(5):1042–1050.
4. Billingham J. Nonlinear sloshing in zero gravity. *J. Fluid Mech.* 2002; **464**:365–391.
5. Socolan YM. Some aspects of the flip-through phenomenon: A numerical study based on the desingularized technique. *Journal of Fluids and Structures* 2010; **26**(6):918 – 953, doi:10.1016/j.jfluidstructs.2010.06.002. URL <http://www.sciencedirect.com/science/article/pii/S088997461000071X>.
6. Shin S, Sohn S, Hwang W. Simple and efficient numerical methods for vortex sheet motion with surface tension. *Int. J. Num. Meth. Fluids* 2014; **74**:422–438.
7. Baker GR, Meiron DI, Orszag SA. Generalized vortex methods for free-surface flow problems. *J. Fluid Mech.* 1982; **123**:477–501.
8. Baker GR, Xie C. Singularities in the complex physical plane for deep water waves. *J. Fluid Mech.* 2011; **685**:83–116, doi:10.1017/jfm.2011.283. URL <http://dx.doi.org/10.1017/jfm.2011.283>.
9. Fontelos M, De La Hoz F. Singularities in water waves and the rayleigh-taylor problem. *J. Fluid Mech.* 2010; **651**:211–239.
10. Kellogg OD. *Foundations of potential theory*. Reprint from the first edition of 1929. Die Grundlehren der Mathematischen Wissenschaften, Band 31, Springer-Verlag: Berlin, 1967.
11. Jaswon MA, Symm GT. *Integral equation methods in potential theory and elastostatics*. Academic Press [Harcourt Brace Jovanovich Publishers]: London, 1977. Computational Mathematics and Applications.
12. Fornberg B. *A practical guide to pseudospectral methods*, *Cambridge Monographs on Applied and Computational Mathematics*, vol. 1. Cambridge University Press: Cambridge, 1996.
13. Clenshaw CW, Curtis AR. A method for numerical integration on an automatic computer. *Numer. Math.* 1960; **2**:197–205.
14. Baker GR, Im JS. Shallow water waves and the korteweg-de vries approximation. *submitted* 2015; .
15. Needham D, Chamberlain P, Billingham J. The initial development of a jet caused by fluid, body and free-surface interaction. part 3. an inclined accelerating plate. *QJMAM* 2008; **61**:581–614.